Int. J. Electrochem. Sci., 10 **(2015)** 10199- 10209

International Journal of
ELECTROCHEMICAL
SCIENCE
www.electrochemsci.org

EQCM Study on Pulse Current Pt Electrodeposition

I-Te Lu[1], Yu-Chi Hsieh[2], Po-Chun Chen[1,3,] and Pu-Wei Wu[1,*]*

[1]Department of Materials Science and Engineering, National Chiao Tung University, Hsinchu 30010, Taiwan
[2]Brookhaven National Laboratory, Chemistry Department, Building 555, Upton, NY 11973, USA
[3]Biomedical Electronics Translational Research Center, National Chiao Tung University, Hsinchu 30010, Taiwan
[*]E-mail: pcchen@g2.nctu.edu.tw; ppwu@mail.nctu.edu.tw

Received: 4 August 2015 / *Accepted:* 18 September 2015 / *Published:* 4 November 2015

Electrochemical Quartz Crystal Microbalance (EQCM) was used to investigate the events occurring during current-on (T_{on}) and current-off (T_{off}) for pulse current electrodeposition of Pt in both air and Ar atmospheres. The EQCM profiles indicated a transient mass loss when the current was turned on, followed by a linear mass gain associated with the Pt electrodeposition from the H_2PtCl_6 plating bath. During the T_{off}, the mass revealed a steady increase until it leveled off after 10 sec. The minute transient mass loss during the initial stage of T_{on} was attributed to the reduction of the adsorbed $PtCl_6^{2-}$ whereas the mass gain during the T_{off} was due to the absorption of $PtCl_6^{2-}$ onto the freshly-deposited Pt surface. In air atmosphere, the parasitic oxygen reduction reaction consumed part of the reduction current and thus, reduced the Pt plating efficiency by 6%. In addition, smaller mass gains during T_{off} and T_{on} were observed for the Pt plating in air atmosphere.

Keywords: Pulse Current Electrodeposition, EQCM, Platinum, Electrodeposition Efficiency

1. INTRODUCTION

Pt is a noble metal known for catalytic activities toward a variety of chemical and electrochemical reactions. [1-4] In electrochemical systems, the Pt reveals desirable attributes in corrosion resistance and exchange current density. [5] For example, in polymer electrolyte fuel cells, the Pt is used for the oxidation of hydrogen at the anode and the reduction of oxygen at the cathode. [6-9] In general, the catalytic performance of Pt depends on its composition, morphology, and surface structure. In the literatures, Pt in cubic, tetrahedral, and cubotahedral shapes has been synthesized and evaluated for catalytic performances. [10-12] So far, the widely used methods to synthesize Pt are chemical reduction and electrodeposition. The chemical reduction route is often employed to form Pt

in nanoparticular forms. For electrochemical application, however, the most straightforward approach is to electroplate the Pt directly onto the current collector because the electrodeposition enables the formation of Pt at the surface so the catalyst utilization rate can be significantly enhanced. [13-16]

The electrodeposition can be conducted in direct-current or pulse mode. Between these two, the pulse mode allows for multiple events of nucleation and growth, as well as sufficient resting time to replenish the electrolyte. To date, the pulse plating technique has been demonstrated for depositing materials within sub-micrometer trenches and producing deposits in unique shapes. [17-19] In pulse electrodeposition, independent parameters, such as current density (J_a), current-on time (T_{on}), and current-off time (T_{off}) are adjusted to obtain deposits with different particle sizes and distributions. [20, 21] In addition, the events occurring during T_{on} and T_{off} play significant roles in determining the deposit morphology and coulombic efficiency. For example, Chen et al. studied the current efficiency under various pulse current conditions and observed a significant morphology change by simply adjusting the T_{on} in Pb/Sn plating bath. [22] It is anticipated that the chemical species in the plating bath or produced during T_{on} would adsorb and interact with the freshly-deposited metal surface during T_{off}, and thus participates in the reduction reaction during subsequent T_{on}.

The electrochemical quartz crystal microbalance (EQCM) is a powerful tool to investigate the events occurring at the working electrode. The operation principle of EQCM and the critical factors affecting the EQCM data have been reviewed in details. [23-25] The EQCM detects the change in the resonance frequency of the working electrode during electrochemical reaction, and correlated the frequency change to the variations in the mass of the deposit, the viscosity of the electrolyte, and temperature. [26-28] Based on the information obtained via EQCM, relevant electrochemical steps can be identified and analyzed, such as electrodeposition, dissolution, adsorption/desorption, and coulombic efficiency. [29-34] In the case of electroplating, the mass change can be determined using the Sauerbrey equation. [35] In short, the mass change caused by the chemical and physical reactions on the working electrode can be monitored in-situ, along with the corresponding potential or current. The mass sensitivity of the EQCM is in the order of ng/cm^2 and therefore, even a subdued mass change on the electrode surface can be detected accurately.

Earlier, the EQCM has been utilized to study the electrodeposition of Pt using potential-controlled methods such as constant potential, pulse potential, and cyclic voltammetric (CV) scans. [25, 36-41] However, none of them discussed the electroplating behavior using pulse galvanostatic deposition via EQCM. In this study, we employed the EQCM to investigate the events occurring during pulse current Pt electrodeposition in both air and Ar atmospheres. The EQCM recorded the variations in mass and potentials during T_{on} and T_{off} in order to identify the chemical reductions, adsorption/desorption, and the role of dissolved oxygen.

2. EXPERIMENTAL

The EQCM instrument consisted of a Research Quartz Crystal Microbalance (RQCM; INFICON) and a potentiostat (VersaSTAT 4; Princeton Applied Research). The resolutions of the RQCM and the potentiostat were 50 and 10 ms per data point. The working electrode was a standard 9

MHz polished Au-coated AT-cut quartz crystal (INFICON) with a geometric area of 1 cm^2. The Ag/AgCl and Pt foil (8 cm^2) were served as the reference and counter electrodes, respectively. The distance between the working electrode and the counter electrode was 6 cm, and the volume of the electrolyte was 100 ml.

Prior to the EQCM calibration and Pt electrodeposition, the working electrode was subjected to multiple CV scans between -0.4 and 1.2 V (vs. Ag/AgCl) in a 0.1 M aqueous H_2SO_4 solution at a scan rate of 50 mV/s. The purpose of the CV scans was to remove any contaminant on the Au surface. Subsequently, the sensitivity of the working electrode was determined using a mixture of 0.01 M $AgNO_3$ and 0.5 M HNO_3 aqueous solutions in which a potentiostatic plating at 50 mV (vs. Ag/AgCl) was conducted for 5 sec. The plating of Ag produced a minute weight increment which resulted in a slight reduction of the resonance frequency of the quartz crystal. The Ag plating was repeated for five consecutive times and assuming its coulombic efficiency was 100%, the sensitivity factor for the Au-coated quartz crystal was 5.799 ng/Hz·cm^2, based on the Saubrey equation. After the calibration, the working electrode was immersed in a 0.1 M aqueous H_2SO_4 solution for multiple CV scans from -0.4 to 1.2 V (vs. Ag/AgCl) at 50 mV/s until the resonance frequency remained unchanged. At this stage, the deposited Ag was stripped completely from the Au surface.

The Pt plating electrolyte was prepared by dissolving 99.9 wt% H_2PtCl_6 (UniRegion Bio-Tech) in deionized water. The resulting concentration was 10 mM and the pH value of the electrolyte was 1.78. The Pt electrodeposition was performed in both air and Ar atmospheres. For the experiments in Ar atmosphere, the plating bath was purged with Ar for 1 hr to remove any dissolved oxygen, and the electrodeposition was carried out in a sealed system saturated with Ar. The Pt electrodeposition was conducted in a pulse current mode in which the current density was -5 mA/cm^2, the T_{on} was 1 sec, and the T_{off} was 50 sec. In total, 20 pulses were imposed and their corresponding variations in mass and potentials were recorded. All the electrochemical process was conducted at 25°C, and the electrolyte was unstirred throughout the entire experiments. Since the pH of the Pt plating bath was 1.78, the potential for the reversible hydrogen electrode (RHE) became -0.305 V (vs. Ag/AgCl) as RHE = [-0.200－0.0591×(pH)]. All the potentials in the figures were plotted against the RHE.

3. RESULTS AND DISCUSSION

The OCV for the working electrode in the Pt plating bath was 1.058 V (vs. RHE). This value reflected the interfacial structure between the Au surface and the Pt ions in the electrolyte. Once the pulse plating was performed, and the Au surface was fully covered by the Pt deposit (after 1 pulse), the OCV became 0.981 V (vs. RHE). Fig. 1(a) displays the EQCM results from pulses #5~#9 for the Pt electrodeposition in air atmosphere. Among these pulses, the OCV at T_{off} maintained a constant value and a sharp drop to -0.272 V was observed once the current was switched on. This indicated a potential drive of 1.253 V for the reduction reaction. During T_{off}, the OCV rose up quickly and continued increasing until it leveled off after 10 sec. As expected, considerable mass gain was recorded during T_{on}, which was attributed to the deposition of Pt from the electrolyte. These EQCM results demonstrated a consistent pattern of successive Pt deposition in every pulse.

Table I. Possible reduction reactions and their respective redox potentials during pulse current electrodepositions (T_{on}) in air atmosphere.

Reduction reaction	Redox potential estimated from Nernst equation (V vs. RHE)[a]	Redox potential in standard state (V vs. RHE)	References
$2H^+ + 2e \rightarrow H_2$	0	0	41
$O_2 + 4H^+ + 4e \rightarrow 2H_2O$	N/A[b]	1.334	41
$PtCl_6^{2-} + 4e \rightarrow Pt + 6Cl^-$	0.819	0.849	41
$PtCl_6^{2-} + 2e \rightarrow PtCl_4^- + 2Cl^-$	N/A[b]	0.831	41
$PtCl_4^{2-} + 2e \rightarrow Pt + 4Cl^-$	N/A[b]	0.863	41

[a] we assume that the activity coefficient is 1 so the value of activity is equal to the concentration.
[b] the exact concentrations of dissolved O_2 and $PtCl_4^{2-}$ are unknown.

Table I lists the possible electrochemical reactions during T_{on} and their corresponding redox potentials. In principle, these reactions were likely to occur to various degrees contingent on their respective concentrations and overpotentials.

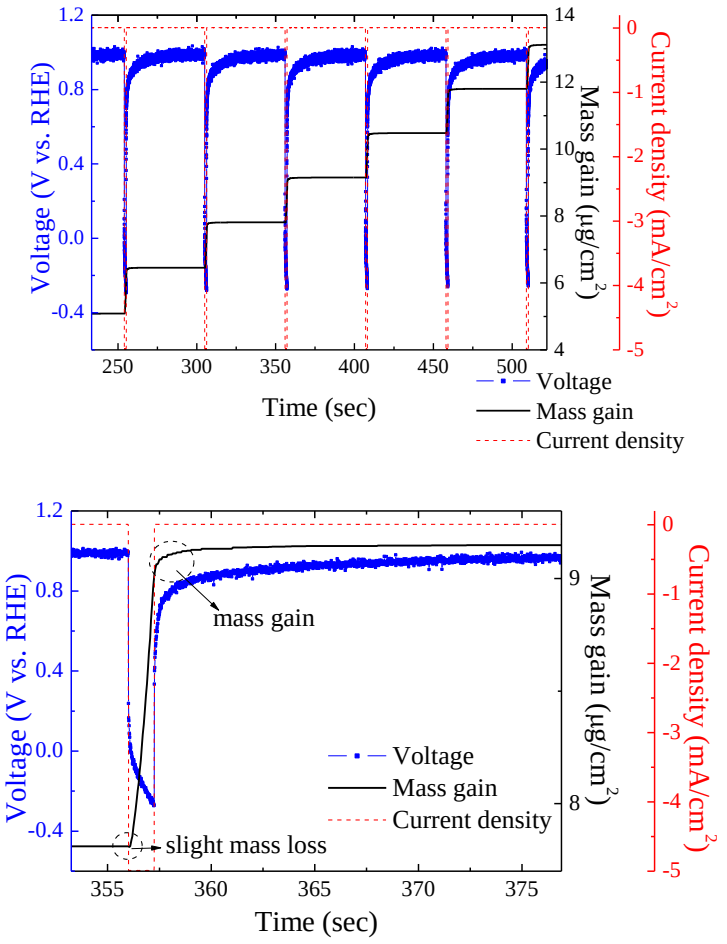

Figure 1. (a) The EQCM profiles from pulses #5~#9 for the Pt electrodeposition in air atmosphere (T_{on} = 1 sec; T_{off} = 50 sec; current density = −5 mA/cm^2). (b) The enlarged EQCM profile from a single pulse (#7).

Fig. 1(b) exhibits the EQCM profile from a single pulse (#7) so the detailed responses of in mass and OCV can be better distinguished. During T_{off}, the OCV reading was 0.981 V. Once the current started flowing (T_{on}), the potential decreased sharply at the beginning, followed by a slow decline. We realized that the former was caused by the double-layer charging and parasitic ohmic drop whereas the latter was associated with the activation and concentration polarizations of possible reactions listed in Table I. Once the current was switched off (T_{off}), the potential rebounded immediately reflecting the removal of ohmic drop. However, the potential continued rising for a few seconds during T_{off}, suggesting the dynamic reconstruction of electrode/electrolyte interface. Table II lists the possible reactions occurring during the initial stages of T_{off} and T_{on}, as well as their expected variations in the mass and OCV.

Table II. Possible reactions during the initial stage of T_{off} and initial stage of T_{on}, as well as their expected variations in the mass and OCV (↓: Decrease; ↑: Increase; —: No change).

	Possible Reactions	Mass	OCV
T_{off}	$PtCl_6^{2-}{}_{(aq)} \rightarrow PtCl_6^{2-}{}_{(ad)}$	↑	↑
	$PtCl_4^{2-}{}_{(aq)} \rightarrow PtCl_4^{2-}{}_{(ad)}$	↑	↑
	$PtCl_6^{2-}{}_{(ad)} + H_{(ad)} \rightarrow Pt$	↓	↓
	$PtCl_4^{2-}{}_{(ad)} + H_{(ad)} \rightarrow Pt$	↓	↓
	$H_{(ad)} + H_{(ad)} \rightarrow H_{2(g)}$	↓	—
	$H_2O_{(aq)} \rightarrow H_2O_{(ad)}$	↑	—
T_{on}	$PtCl_6^{2-}{}_{(ad)} \rightarrow Pt_{(s)}$	↓	
	$PtCl_4^{2-}{}_{(ad)} \rightarrow Pt_{(s)}$	↓	
	$H_2O_{(ad)} \rightarrow H_{(ad)} \rightarrow H_{2(g)}$	↓	
	$H^+_{(aq)} \rightarrow H_{(ad)} \rightarrow H_{2(g)}$	—	
	$O_2 + 4H^+ \rightarrow 2H_2O$	—	

For the mass variation, a slight mass loss was observed during the start of T_{on}, which was due to the reduction of the adsorbed $PtCl_6^{2-}$ on the freshly-deposited Pt surface. Afterwards, a sizeable mass gain was recorded owing to the deposition of Pt from the Pt ions in the electrolyte, i.e., the electrochemical reduction of $PtCl_6^{2-}$ and $PtCl_4^{2-}$. Interestingly, during T_{off}, a moderate mass increment was also recorded which was attributed to the adsorption of $PtCl_6^{2-}$ from the electrolyte. According to earlier studies of Pt (111) film immersed in an aqueous solution containing 0.6 mM H_2PtCl_6 and 50 mM $HClO_4$, the adsorbed species on the Pt (111) surface at potential between 0.7 ~ 0.95 V (vs. RHE) was exclusively $PtCl_6^{2-}$. [42] Therefore, in our case we believed that once the current was turned off, the $PtCl_6^{2-}$ was adsorbed preferentially to the fresh Pt surface, leading to a steady rise of the OCV to 0.981 V (vs. RHE). It is noted that this 0.981 V was more positive than the redox potential of $PtCl_6^{2-}$/Pt which was 0.819 V (vs. RHE) for 10 mM H_2PtCl_6 electrolyte from Nernst equation. Hence, thermodynamics favored the formation and stability of $PtCl_6^{2-}$ adsorption onto the fresh Pt surface.

An alternative explanation for the mass gain during T_{off} might be the formation of $Pt(OH)_x$ or the adsorption of Cl^- ions. In the literatures, the Pt surface was prone to form $Pt(OH)_x$ at potential up to 0.85 V (vs. RHE) in acidic solutions. [43, 44] In our case, the OCV during T_{off} was 0.981 V (vs. RHE),

and thus the presence of $Pt(OH)_x$ was likely. However, the H_2PtCl_6 was not used in those studies but in our plating bath the $PtCl_6^{2-}$ was the predominant constituent. In theory, the mass gain associated with the $Pt(OH)_x$ during T_{off} should be equal to the transient mass loss during T_{on} because the reduction current was expected to reduce the adsorbed species first. However, in our case the EQCM profiles indicated a different pattern; the transient mass loss during T_{on} was merely 13% of the mass gain during T_{off}. Therefore, we concluded that the formation of $Pt(OH)_x$ was not the principal contributor to the mass gain during T_{off}. Likewise, the amount of adsorbed Cl^- during T_{off} was likely to be relatively low. It is also possible that during T_{off}, the adsorbed hydrogen engaged in a displacement reaction with the $PtCl_6^{2-}$ ions from the electrolyte, resulting in a mass gain. However, according to Solla-Gullon et al. and Nutariya et al., the adsorbed hydrogen can only exist on the fresh Pt surface in a potential range between 0.12 and 0.27 V (vs. RHE). [45] Therefore, we concluded that the mass gain during T_{off} was not caused by the formation of $Pt(OH)_x$, the adsorption of Cl^-, and the displacement reaction of the adsorbed hydrogen.

The Pt is an electrocatalyst for oxygen reduction reaction (ORR) and the pulse plating inevitably induces the ORR in conjunction with the deposition of Pt.

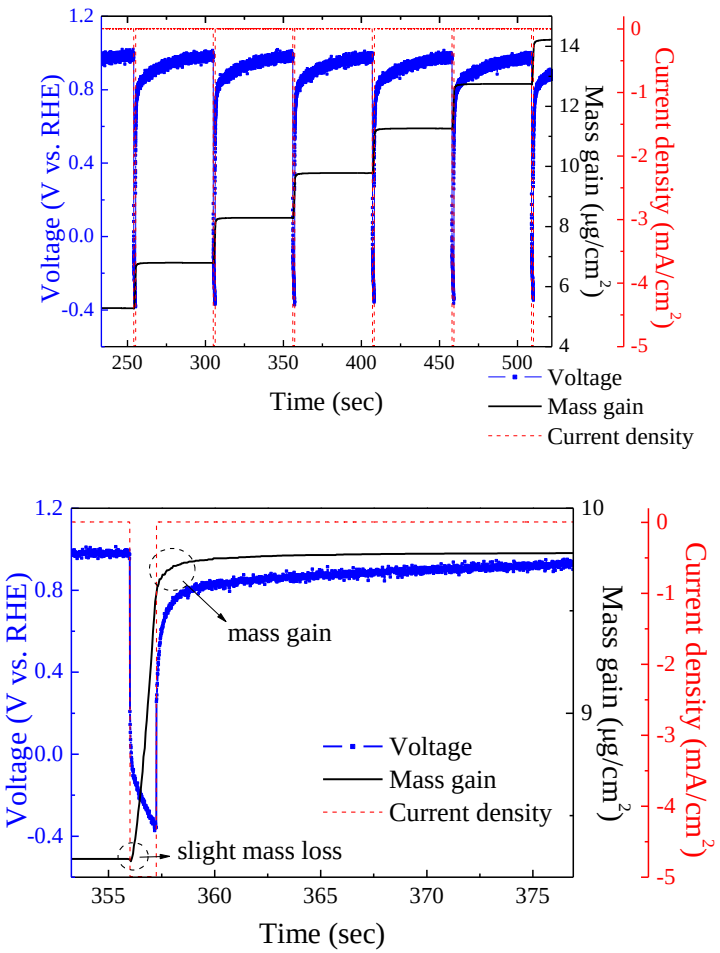

Figure 2. (a) The EQCM profiles from pulses #5~#9 for the Pt electrodeposition in Ar atmosphere (T_{on} = 1 sec; T_{off} = 50 sec; current density = −5 mA/cm^2). (b) The enlarged EQCM profile from a single pulse (#7).

To investigate the effect of dissolved oxygen in the electrolyte, we performed the EQCM experiments in deaerated bath. Fig. 2(a) displays the EQCM results from pulses #5~#9 for the Pt electrodeposition in Ar atmosphere. In general, the EQCM results were rather similar to those shown in Fig. 1(a). The OCV at T_{off} was 0.981 V (vs. RHE), and the potential experienced a sharp drop when the current was turned on. Likewise, during T_{on}, a transient mass loss was observed followed by a notable mass gain. Once the current was switched off, both the OCV and mass continued increasing and leveled off after 10 sec. Fig. 2(b) shows an enlargement of pulse #7 which revealed a similar pattern as that of Fig. 1(b).

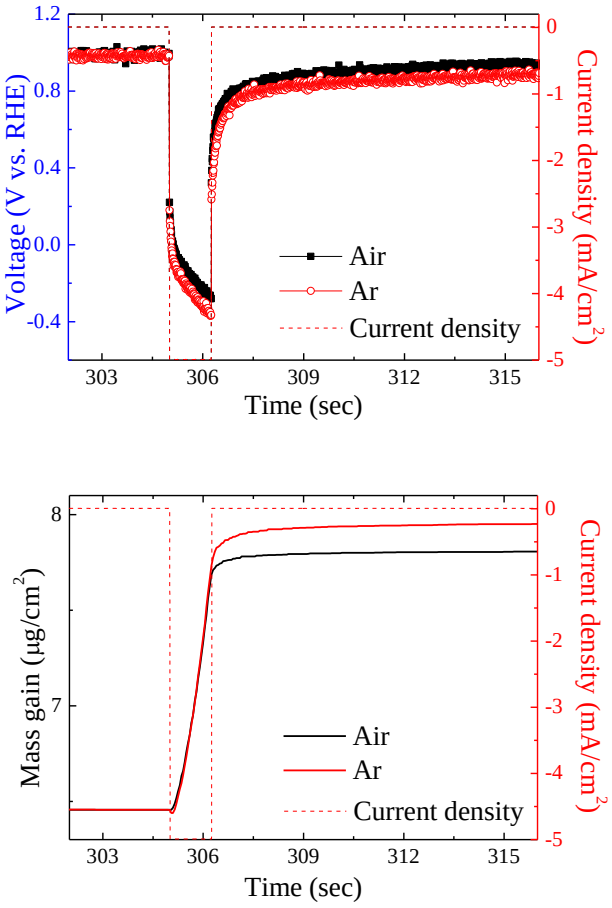

Figure 3. Comparison of EQCM profiles from pulse #7 in air and Ar atmospheres; (a) voltage vs. time, and (b) mass gain vs. time.

Fig. 3 provides the EQCM profiles in potentials and mass gains from the pulse #7 in both air and Ar atmospheres, respectively. As shown in Fig. 3(a), the OCVs during T_{off} in both samples exhibited values of 0.981 V (vs. RHE), suggesting identical electrode/electrolyte structures. During T_{on}, their potentials revealed an instantaneous drop to 0.221 V, and became increasingly negative with plating time. In a galvanostatic mode, the potential response can be explained by chronopotentiometric behavior in which the flux of $PtCl_6^{2-}$ at the electrode surface (x = 0) can be deduced at any given time by the Fick's first law;

$$J_o(x,t) = -D_o \frac{\partial C_o(x,t)}{\partial t} = \frac{i(t)}{nFA} \quad (1)$$

where the J_0 is the flux of $PtCl_6^{2-}$ toward the working electrode, the D_0 is the diffusion coefficient of $PtCl_6^{2-}$ in the plating bath, the A is the microscopic area of the deposited Pt, the F is the Faraday's constant, and the $i(t)$ is the input current. Because the $i(t)$ was kept constant, the flux or the concentration gradient at the working electrode surface remained unchanged throughout the plating process. This behavior agreed well with the linear mass gain shown in Fig. 1(b) and Fig. 2(b).

The concentration of $PtCl_6^{2-}$ at the working electrode surface ($C_0(0,t)$) can be obtained by the following equation; [46]

$$C_o(0,t) = C_o^* - \frac{2it^{1/2}}{nFAD_o^{1/2}\pi^{1/2}} \quad (2)$$

where the C_o^* is the bulk concentration of $PtCl_6^{2-}$, and the t is the plating time. According to equation (2), the $C_0(0,t)$ was expected to fall steadily with plating time. Because the mass increased linearly during T_{on}, a constant deposition rate was anticipated. Therefore, the $C_0(0,t)$ did not fall to zero; if the $C_0(0,t)$ did fall to zero, the potential was expected to drop significantly to a more negative value in order to initiate an alternative reduction reaction. It is realized that the potential was related to the surface concentration of $PtCl_6^{2-}$, as dictated by the Nernst equation. Because of the steady reduction in the surface $PtCl_6^{2-}$ concentration as plating time progressed during T_{on}, the potential became increasingly negative, a typical behavior known as concentration polarization. As shown in Fig. 3(a), the potential drop in air atmosphere was relatively smaller as compared to that in Ar atmosphere. This inferred that at any given time the surface concentration of $PtCl_6^{2-}$ in air atmosphere was higher. We realized that in air atmosphere part of the reduction current was consumed by the ORR which was facilitated by the presence of freshly-deposited Pt. This led to a relatively slow decrease in the concentration of surface $PtCl_6^{2-}$. The occurrence of ORR also reduced the coulombic efficiency and as a result, rendered a smaller amount of Pt deposition in air atmosphere, as shown in Fig. 3(b). During the T_{off}, the OCV rose faster in air atmosphere because of the relatively abundant $PtCl_6^{2-}$ on the surface. This produced a more positive potential as predicted by the Nernst equation.

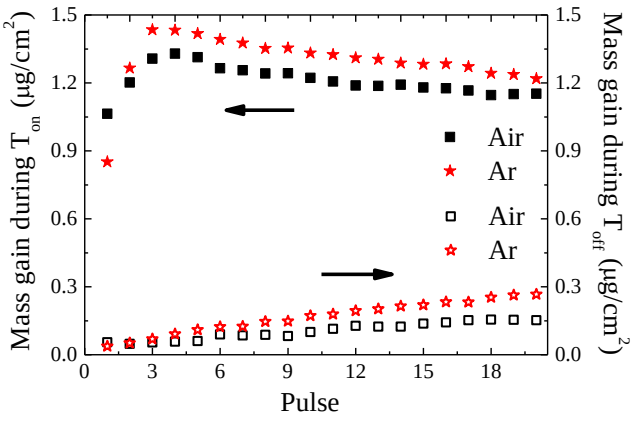

Figure 4. The amount of mass gain for 20 consecutive pulses during T_{on} and T_{off} in both air and Ar atmospheres.

Fig. 4 demonstrates the amount of mass gain for 20 consecutive pulses during T_{on} and T_{off} in both air and Ar atmospheres, respectively. To cover the entire Au surface, the necessary Pt amount was 0.484 μg/cm^2 for a monolayer of Pt (111). Therefore, from the mass gain during T_{on}, the Au surface was fully covered by the Pt after the first pulse, which was consistent with the OCV observation during T_{off}. For both samples, the mass gains during T_{on} were much greater than those during T_{off}. In addition, the mass gain during T_{on} in Ar atmosphere was consistently larger than that in air because the absence of dissolved oxygen for the ORR in the latter case. On the other hand, the mass gain due to the adsorption of $PtCl_6^{2-}$ was larger in Ar atmosphere than that in air atmosphere. Except for the first few pulses, the amount of mass gain during T_{on} for both samples exhibited a decreasing trend whereas the mass gain due to the surface $PtCl_6^{2-}$ adsorption revealed an opposite pattern. We believed that an increasing microscopic surface area of the Pt with increasing pulses allowed for more adsorption of $PtCl_6^{2-}$. The adsorbed $PtCl_6^{2-}$ was subsequently reduced when the current was turned on, so the current left for reducing the $PtCl_6^{2-}$ in the electrolyte became less and the amount of Pt deposit became smaller with increasing pulses.

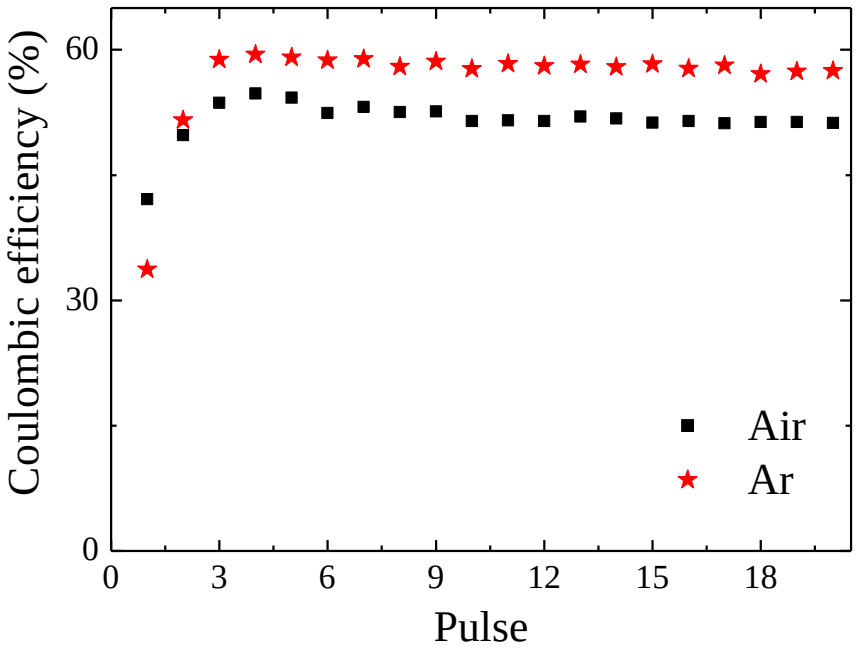

Figure 5. The coulombic efficiencies of Pt deposition during T_{on} for both air and Ar atmospheres.

Fig. 5 exhibits the coulombic efficiencies of Pt deposition during T_{on} for both air and Ar atmospheres. The coulombic efficiencies in Ar case were consistently larger than those in air. Except for the first few pulses, the coulombic efficiencies were around 52% in air whereas in Ar case the coulombic efficiencies were improved to 58%. It was therefore concluded that approximate 6% of the pulse current was consumed by the ORR, and the remaining 40% pulse current was utilized to reduce

$PtCl_6^{2-}$ to $PtCl_4^{2-}$, and engaged in the parasitic hydrogen evolution reaction. It is noted that the $PtCl_4^{2-}$ was not adsorbed on the working electrode and hence was not responsible for the mass loss during T_{on}.

4. CONCLUSION

The EQCM was utilized to study the events occurring during T_{on} and T_{off} in pulse current electrodeposition of Pt. For both air and Ar atmospheres, during T_{on}, the EQCM profiles indicated a transient mass loss, followed by a linear mass gain. The transient mass loss was caused by the reduction of the adsorbed $PtCl_6^{2-}$ whereas the linear mass gain was associated with the Pt plating from the electrolyte. During T_{off}, the mass revealed a steady increase until it leveled off after 10 sec which was due to the absorption of $PtCl_6^{2-}$ onto the freshly-deposited Pt surface. In air atmosphere, the parasitic ORR reduced the Pt plating efficiency by 6%. In addition, smaller mass gains during T_{off} and T_{on} were observed for the Pt plating in air atmosphere.

ACKNOWLEDGEMENT
This work was fully supported by the Taiwan Ministry of Science and Technology under grant numbers (MOST-104-2220-E-009-005), and in part by "Aim for the Top University Plan" of the National Chiao Tung University and Ministry of Education, Taiwan, R.O.C.

References

1. P. Mathew, J.P. Meyers, R. Srivastava, P. Strasser, *Journal of the Electrochemical Society*, 159 (2012) B554-B563.
2. F. Takasaki, S. Matsuie, Y. Takabatake, Z. Noda, A. Hayashi, Y. Shiratori, K. Ito, K. Sasaki, J*ournal of the Electrochemical Society*, 158 (2011) B1270-B1275.
3. K.-W. Park, J.-H. Choi, B.-K. Kwon, S.-A. Lee, Y.-E. Sung, H.-Y. Ha, S.-A. Hong, H. Kim, A. Wieckowski, *The Journal of Physical Chemistry B*, 106 (2002) 1869-1877.
4. J. Solla-Gullon, F. Vidal-Iglesias, A. Lopez-Cudero, E. Garnier, J. Feliu, A. Aldaz, *Physical Chemistry Chemical Physics*, 10 (2008) 3689-3698.
5. J. Zhang, PEM fuel cell electrocatalysts and catalyst layers: fundamentals and applications, Springer, 2008.
6. M. Croissant, T. Napporn, J.-M. Léger, C. Lamy, *Electrochimica Acta*, 43 (1998) 2447-2457.
7. N. Marković, T. Schmidt, V. Stamenković, P. Ross, *Fuel Cells*, 1 (2001) 105-116.
8. C. Wang, H. Daimon, Y. Lee, J. Kim, S. Sun, *Journal of the American Chemical Society*, 129 (2007) 6974-6975.
9. J. Zhang, M.B. Vukmirovic, K. Sasaki, A.U. Nilekar, M. Mavrikakis, R.R. Adzic, *Journal of the American Chemical Society*, 127 (2005) 12480-12481.
10. K.M. Bratlie, H. Lee, K. Komvopoulos, P. Yang, G.A. Somorjai, *Nano Letters*, 7 (2007) 3097-3101.
11. R. Narayanan, M.A. El-Sayed, *Journal of the American Chemical Society*, 126 (2004) 7194-7195.
12. R. Narayanan, M.A. El-Sayed, *Nano Letters*, 4 (2004) 1343-1348.
13. S.D. Thompson, L.R. Jordan, M. Forsyth, *Electrochimica Acta*, 46 (2001) 1657-1663.
14. A. Mikhaylova, O. Khazova, V. Bagotzky, *Journal of Electroanalytical Chemistry*, 480 (2000) 225-232.
15. F. Gloaguen, J.-M. LE, C. Lamy, *Journal of Applied Electrochemistry*, 27 (1997) 1052-1060.
16. M. Shaddad, A. Al-Mayouf, M. Ghanem, M. AlHoshan, J. Singh, A. Al-Suhybani, *International*

Journal of Electrochemical Science, 8 (2013) 2468-2478.
17. P. Dixit, J. Miao, *Journal of the Electrochemical society*, 153 (2006) G552-G559.
18. N. Qu, D. Zhu, K. Chan, W. Lei, *Surface and Coatings Technology*, 168 (2003) 123-128.
19. J. Zhu, S. Liu, O. Palchik, Y. Koltypin, A. Gedanken, *Langmuir*, 16 (2000) 6396-6399.
20. S.-S. Kim, Y.-C. Nah, Y.-Y. Noh, J. Jo, D.-Y. Kim, *Electrochimica Acta*, 51 (2006) 3814-3819.
21. J.A. Bennett, Y. Show, S. Wang, G.M. Swain, *Journal of the Electrochemical society*, 152 (2005) E184-E192.
22. C. Chen, C. Wan, *Journal of the Electrochemical society*, 136 (1989) 2850-2855.
23. A. Arnau, *Sensors*, 8 (2008) 370-411.
24. D.A. Buttry, M.D. Ward, *Chemical Reviews*, 92 (1992) 1355-1379.
25. S. Nilsson, F. Björefors, N.D. Robinson, *Applied Surface Science*, 280 (2013) 783-790.
26. D. Wang, P. Mousavi, P.J. Hauser, W. Oxenham, C.S. Grant, *Colloids and Surfaces* A: *Physicochemical and Engineering Aspects*, 268 (2005) 30-39.
27. D.Y. Ryu, M.L. Free, *Journal of colloid and interface science*, 264 (2003) 402-406.
28. A. StankeviČiu, K. Leinartas, G. BikulČius, D. VirbalytĖ, A. SudaviČius, E. Juzeliu, J*ournal of applied electrochemistry*, 28 (1998) 89-95.
29. T.L. Knutson, W.H. Smyrl, *Journal of the Electrochemical society*, 154 (2007) B1095-B1099.
30. Y. Hussain, Y.-T. Wu, P.-J. Ampaw, C.S. Grant, *The Journal of supercritical fluids*, 42 (2007) 255-264.
31. K. Wang, H. Pickering, K. Weil, *Electrochimica Acta*, 46 (2001) 3835-3840.
32. M. Santos, D. Miwa, S. Machado, *Electrochemistry communications*, 2 (2000) 692-696.
33. H.-W. Lei, H. Uchida, M. Watanabe, *Langmuir*, 13 (1997) 3523-3528.
34. Z. Nováková, R. Oriňáková, A. Oriňák, P. Hvizdoš, A.S. Fedorková, *International Journal of Electrochemical Science*, 9 (2014) 3846-3863.
35. M.R. Deakin, D.A. Buttry, *Analytical Chemistry*, 61 (1989) 1147A-1154A.
36. Y. Liu, D. Gokcen, U. Bertocci, T.P. Moffat, *Science*, 338 (2012) 1327-1330.
37. H.-F. Waibel, M. Kleinert, L. Kibler, D. Kolb, *Electrochimica Acta*, 47 (2002) 1461-1467.
38. B. Gollas, J.M. Elliott, P.N. Bartlett, *Electrochimica Acta*, 45 (2000) 3711-3724.
39. K. Uosaki, S. Ye, Y. Oda, T. Haba, K.-i. Hamada, *Langmuir*, 13 (1997) 594-596.
40. T.-Y. Chiang, M.-C. Huang, C.-H. Tsai, *Applied Surface Science*, 308 (2014) 293-300.
41. A. Kishi, M. Inoue, S. Shironita, M. Umeda, *Applied Surface Science*, 258 (2012) 7497-7502.
42. K. Uosaki, S. Ye, H. Naohara, Y. Oda, T. Haba, T. Kondo, *The Journal of Physical Chemistry B*, 101 (1997) 7566-7572.
43. B. Conway, *Progress in surface science*, 49 (1995) 331-452.
44. H. Angerstein-Kozlowska, B. Conway, W. Sharp, *Journal of Electroanalytical Chemistry and Interfacial Electrochemistry*, 43 (1973) 9-36.
45. J. Nutariya, M. Fayette, N. Dimitrov, N. Vasiljevic, *Electrochimica Acta*, (2013).
46. A.J. Bard, L.R. Faulkner, (2001).